SPRINGER SERIES IN COMPUTATIONAL NEUROSCIENCE

Analysis of Parallel Spike Trains

Sonja Grün
Stefan Rotter
Editors

Springer

Springer Series in Computational Neuroscience

Volume 7

For further volumes:
http://www.springer.com/series/8164

Sonja Grün • Stefan Rotter
Editors

Analysis of Parallel Spike Trains

Springer

Editors
Sonja Grün
Laboratory for Statistical Neuroscience
RIKEN Brain Science Institute
2-1 Hirosawa
Wakoshi
Saitama 351-0198
Japan
gruen@brain.riken.jp

Stefan Rotter
Bernstein Center Freiburg
& Faculty of Biology
Albert-Ludwig University
Hansastrasse 9a
79104 Freiburg
Germany
stefan.rotter@biologie.uni-freiburg.de

ISBN 978-1-4419-5674-3 e-ISBN 978-1-4419-5675-0
DOI 10.1007/978-1-4419-5675-0
Springer New York Dordrecht Heidelberg London

Library of Congress Control Number: 2010933856

Cover design: The cover artwork (original in oil pastel and acrylic) was designed and created by Adrián Ponce Alvarez.

Printed on acid-free paper

Springer is part of Springer Science+Business Media (www.springer.com)

Chapter 10
Unitary Event Analysis

Sonja Grün, Markus Diesmann, and Ad Aertsen

Abstract It has been proposed that cortical neurons organize dynamically into functional groups ("cell assemblies") by the temporal structure of their joint spiking activity. The Unitary Events analysis method detects conspicuous patterns of coincident spike activity among simultaneously recorded single neurons. The statistical significance of a pattern is evaluated by comparing the number of occurrences to the number expected on the basis of the firing rates of the neurons. Key elements of the method are the proper formulation of the null hypothesis and the derivation of the corresponding count distribution of coincidences used in the significance test. Performing the analysis in a sliding window manner results in a time-resolved measure of significant spike synchrony. In this chapter we review the basic components of UE analysis and explore its dependencies on parameters like the allowed temporal imprecision and features of the data like firing rate and coincidence rate. Violations of the assumptions of stationarity of the firing rate within the analysis window and Poisson statistics can be tolerated to a reasonable degree without inducing false positives. We conclude that the UE method is robust already in its basic form. Still, it is preferable to use coincidence distributions for the significance test that are well adapted to particular features of the data. The chapter presents practical advice and solutions based on surrogates.

10.1 Introduction

The principles of neuronal information processing are still not well understood and continue to be debated (Shadlen and Movshon 1999). In the classical view,

S. Grün (✉)
Laboratory for Statistical Neuroscience, RIKEN Brain Science Institute, 2-1 Hirosawa, Wakoshi, Saitama 351-0198, Japan
e-mail: gruen@brain.riken.jp
url: http://www.cnpsn.brain.riken.jp

S. Grün, S. Rotter (eds.), *Analysis of Parallel Spike Trains,*
Springer Series in Computational Neuroscience 7,
DOI 10.1007/978-1-4419-5675-0_10,

firing rates play a central role in neural coding (Barlow 1972). This idea indeed led to fundamental insights into the neuronal mechanisms of brain function. In parallel, however, a different concept was developed, in which the temporal organization of spike discharges within functional groups of neurons, so-called neuronal assemblies (Hebb 1949; Gerstein et al. 1989), contributes to neural coding (Von der Malsburg 1981; Abeles 1991; Singer 1999; Harris 2005). It was argued that the biophysics of synaptic integration favors coincident presynaptic events over asynchronous ones (Abeles 1982; Softky and Koch 1993; Goedeke and Diesmann 2008). Accordingly, synchronized spikes are considered a property of neuronal signals that can be detected and propagated by other neurons (Diesmann et al. 1999). In addition, these spike correlations should be dynamic, reflecting varying affiliations of the neurons, depending on stimulus and behavioral context. Thereby, synchrony of firing would be directly available to the brain as a potential neural code.

Experimental studies provide support for both perspectives, and both coding schemes may well coexist. However, the discussion about the relevant coding scheme is often implicitly a discussion about the analysis methods and their ability to decide between the two. Therefore, there is a need for analysis tools that allow us to reliably detect correlated spiking activity that is not explained by the firing rates of the neurons alone. The Unitary Events (UE) analysis is such a tool. It was designed to detect coordinated spiking activity that occurs significantly more often than predicted by the firing rates of the neurons. The method allows one to analyze correlations not only between pairs of neurons but also between multiple neurons, by considering the various spike patterns across the neurons. In addition, the method allows one to extract the dynamics of correlation between the neurons by performing the analysis in a time-resolved manner. This enables us to relate the occurrence of spike synchrony to behavior.

This chapter reviews first the basic components of the UE method: a significance test based on the null hypothesis of independent firing and the machinery for a time-resolved analysis. Under certain conditions, the analysis can be based on analytical expressions. We use these expressions to discuss the characteristics of the method and demonstrate that the approach copes well with typical features of experimental data (nonstationarities in time and across trials, deviation from Poisson). Subsequently, we discuss solutions based on surrogates that incorporate more complex features of experimental data into the null hypothesis. After relating the UE approach to other correlation analysis methods, we conclude with a practical guideline for data analysis.

10.2 Basic Elements of the UE approach

The UE analysis method (Grün et al. 2002a) is designed to detect coincident spike patterns between two or more simultaneously recorded spike trains and to assess the significance of the observation. The specific questions addressed by this analysis are: (1) do the simultaneously recorded neurons show correlations of their spiking

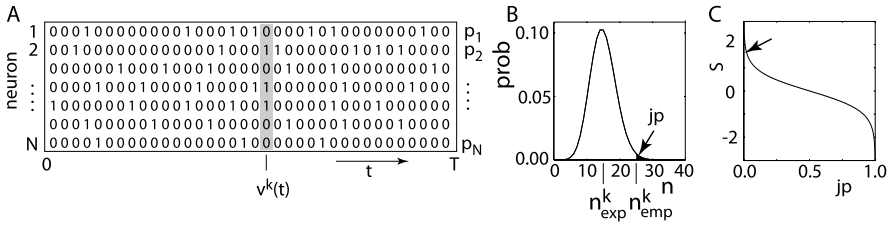

Fig. 10.1 **A**. Binary data representation of N parallel spike trains within a data stretch of T bins of width h. **B**. Distribution of coincidences given the expected number n_{exp}. Significance (jp-value, *black area*) of the number of empirically found coincidences n_{emp}. **C**. Transformation of the jp-value into the surprise measure S. The *arrow* indicates the surprise value corresponding to the identified jp-value in **B**. (Modified from Grün 2009.)

activity, (2) is any such correlation specific to subgroups of the neurons, and (3) do these correlations change dynamically in dependence of stimuli or behavior?

10.2.1 Detection of Joint-Spike Events

The spiking activity of all simultaneously recorded neurons is represented, after appropriate time discretization (e.g., $h = 1$ ms), as parallel sequences of zeros and ones; "1" indicating the existence of at least one spike (clipping), and "0" the absence of spikes (Fig. 10.1A). Under the assumption of stationary firing, the marginal firing probability p_i of neuron i is estimated by evaluating its spike frequency, i.e., the number of ones c_i within the total number of bins T/h in the observed time interval of duration T, and thus, $p_i = c_i/(T/h)$. A similar statistic can be obtained for a particular coincidence pattern composed of zeros and ones. There are at most 2^N different coincidence patterns in data of N simultaneously observed neurons. Due to the finite recording time and the dominance of zeros, however, the actual number of different coincidence patterns found is typically much lower. A unique index k is assigned to each existing pattern based on some arbitrary sorting. For each pattern k, we determine the number of occurrences termed the empirical count n^k_{emp}.

10.2.2 Null Hypothesis

We are interested in detecting whether a coincidence pattern occurs significantly more often than expected on the basis of the firing rates of the neurons involved. To this end, we compare the empirical number of occurrences of pattern k to the expected number by calculating the joint probability of occurrence of the particular 0–1 configuration assuming statistical independence:

$$P^k_{\text{exp}} = \prod_{i=1}^{N} \varphi\left(\overrightarrow{v}(i)\right) \quad \text{with } \varphi\left(\overrightarrow{v}(i)\right) = \begin{cases} p_i & \text{if } \overrightarrow{v}(i) = 1, \\ 1 - p_i & \text{if } \overrightarrow{v}(i) = 0, \end{cases} \tag{10.1}$$

where p_i is the occupation probability of a bin of neuron i.

The expected number of occurrences of pattern k is then simply given by

$$n_{\text{exp}}^k = P_{\text{exp}}^k \cdot \frac{T}{h}.$$

For better readability, we omit from now on the pattern index k but keep in mind that each expression also holds for any pattern k with P_{exp} defined by (10.1).

If multiple trials are available and cross-trial stationarity cannot be guaranteed, the total number of expected coincidences (10.1) is calculated as the sum of the expected counts of the individual trials

$$n_{\text{exp}} = \sum_{j=1}^{M} \frac{T}{h} P_{\text{exp},j} = \sum_{j=1}^{M} \frac{T}{h} \cdot \prod_{i=1}^{N} \varphi_j\left(\overrightarrow{v}(i)\right)$$
$$\text{with } \varphi_j\left(\overrightarrow{v}(i)\right) = \begin{cases} \frac{c_{i,j}}{T/h} & \text{if } \overrightarrow{v}(i) = 1, \\ 1 - \frac{c_{i,j}}{T/h} & \text{if } \overrightarrow{v}(i) = 0, \end{cases} \tag{10.2}$$

where $c_{i,j}$ is the count for neuron i in trial j. In case we can assume stationarity across trials within T, the firing probabilities of the neurons can be derived as averages across the M trials $p_i = \frac{1}{M} \sum_{j=1}^{M} \frac{c_{i,j}}{T/h}$. The empirical coincidence count is the sum of the coincidences found in the individual trials, $n_{\text{emp}} = \sum_{j=1}^{M} n_{\text{emp},j}$.

10.2.3 Significance of Joint-Spike Events

Next, we evaluate whether the empirical number of coincidences significantly deviates from the expected number. To this end we test if the number of empirical coincidences is consistent with the coincidence distribution resulting from independent processes. The probability P_{exp} to observe pattern k in a particular bin is typically low because already the contributing spikes have a low probability of occurrence. As P_{exp} holds for all bins of the analysis interval, the observed number of patterns is governed by a binomial distribution. For moderate n_{exp}, it is well approximated by a Poisson distribution $\mathscr{P}(n, n_{\text{exp}})$ with n_{exp} as the sole parameter. Note that this distribution ignores any dependencies between the bins. For example, there is a finite probability for n occurrences of a pattern requiring a spike of a particular neuron, even if n exceeds the total number of bins in the interval or the number of spikes the neuron has generated. Similarly, any interval statistics of the spike generation process deviating from Poisson leads to correlation between the bins. More complex analytical distributions can take some of these boundary conditions into account (see Grün et al. 2002a, 2003). Here we use the Poisson distribution because the closed-form expression enables us to illustrate the construction of the significance test and its main characteristics. In Sect. 10.4 we show that the Poisson distribution is also of practical use because it is quite robust against typical violations of the simple assumption that spike trains are generated by a Poisson process with constant rate. In later sections we argue that the large diversity of the experimental data

suggests the generation of count distributions employing the idea of surrogate data rather than the use of explicitly parameterized analytical expressions.

Based on the count distribution $\mathscr{P}$, we define the significance of the empirical number of coincidences n_{emp} as the p-value (here called joint-p-value, jp), i.e., the probability of observing at least n_{emp} coincidences (Fig. 10.1B):

$$\begin{aligned} \text{jp}(n_{\text{emp}}|n_{\text{exp}}) &= \sum_{n=n_{\text{emp}}}^{\infty} \mathscr{P}(n_{\text{emp}}, n_{\text{exp}}) \\ &= \sum_{n=n_{\text{emp}}}^{\infty} \frac{(n_{\text{exp}})^n}{n!} \cdot \exp(-n_{\text{exp}}). \end{aligned} \tag{10.3}$$

If jp is smaller than a predefined significance level α, we infer excess synchrony. If jp is larger than $1-\alpha$, we infer significantly missing coincidences. If excess is detected for the respective coincidence pattern, we call the instantiations of the spike patterns Unitary Events (UE).

Because highly significant events are indicated by very small jp values, we logarithmically transform the jp value into the surprise measure (Palm 1981) for better visualization (Fig. 10.1C):

$$S(\text{jp}) = \log \frac{1-\text{jp}}{\text{jp}}. \tag{10.4}$$

This measure is zero for no deviation from expectation, positive in the presence of more coincidences than expected, and negative if the measurement is lower than the expected count. Large values of S indicate significance (e.g., significance at the 1% level results in a surprise measure of 2.0).

10.2.4 Capturing Dynamics of Correlation

In order to capture time dependent changes of the correlation between neurons, we formulate a time-resolved version of the UE analysis defined in the previous section, using a sliding-window approach. To improve the statistics, neuronal data are typically recorded multiple times under the same stimulus presentation or the same behavioral condition ("trials"). The underlying assumption is that the same neuronal computation is performed across the trials. Therefore, data are cut into trials and aligned on the corresponding stimulus or behavioral event. Then we decide on the width T_{w} (expressed in the number of bins h) of a time window which we slide along the data (Fig. 10.2). At each window position, we separately carry out the UE analysis restricted to this window and simultaneously for all trials (Grün et al. 2002b).

The result of the analysis of a window is represented at the center of the window. The time series of results from subsequent windows provides us with a time-resolved analysis. The offset of successive sliding window positions defines the time resolution of the analysis. For each pattern k, the empirical and

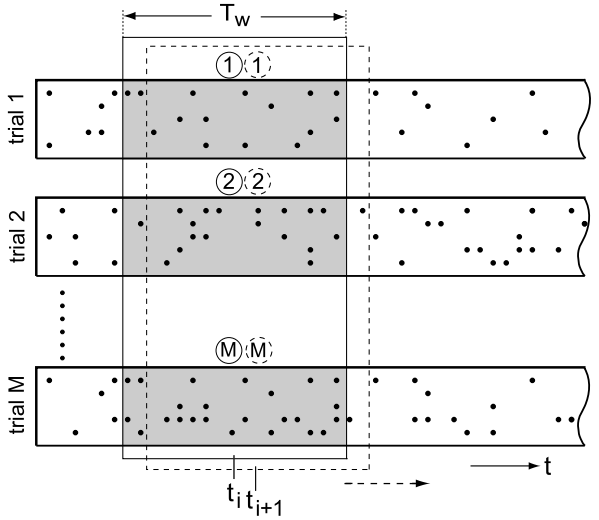

Fig. 10.2 Capturing correlation dynamics by sliding window analysis. After alignment of trials, a window of size T_w is slid along time. At each position of the window, the time segments of all trials covered by the window (*gray*, indicated by *circled trial numbers* from $1, \ldots, M$) are extracted and analyzed for UEs. The procedure is repeated at each new position of the sliding window. The results of each sliding window position are represented at the center of the window, thereby deriving time dependent measures. (Modified from Grün et al. 2002b.)

expected numbers of coincidences are obtained as functions of time ($n_{exp}(t)$, $n_{emp}(t)$, Fig. 10.3B), and the significance is expressed by the surprise measure $S(t)$ (Fig. 10.3C). Thus, the approach enables us to directly relate the dynamics of synchrony (Fig. 10.3D) to the dynamics of the stimulation or the specific behavior of the animal (Riehle et al. 1997, 2000; Grammont and Riehle 2003; Maldonado et al. 2008). In addition, by observing the time-dependent modulation of the occurrence of the different joint-spike patterns we can draw conclusions on the composition of currently active assemblies and the respective participation of the recorded neurons (Grammont and Riehle 1999).

Unitary Event computation

1. Align trials, decide on width of analysis window.
2. Decide on allowed coincidence width.
3. Perform a sliding window analysis. In each window:
   a. Detect and count coincidences.
   b. Calculate expected number of coincidences.
   c. Evaluate significance of detected coincidences.
   d. If significant, the window contains Unitary Events.
4. Explore behavioral relevance of UE epochs.

10.3 Parameter Dependencies

10.3.1 Analysis Window Width

The time scales of the change in firing rate and the modulation of the rate of coincidence events can differ. Even for a temporally stationary firing rate, synchrony may be modulated on a time scale of tens or hundreds of milliseconds (e.g., Vaadia et al. 1995). The UE uses a sliding-window approach to capture such modulation of synchrony (Fig. 10.3). The proper choice of the sliding window width required to identify excess synchrony as significant depends on two factors, the width of the time interval T_c containing excess synchrony ("hot region") and the rate of coincidences λ_c relative to the independent background rate. In the following we analytically study an injection model where coincidences of rate λ_c are injected into independent background activity of rate λ_b in a predefined time interval, yielding a total rate of $\lambda = \lambda_c + \lambda_b$. The background activity is adjusted so that the total rate λ exactly matches the spike rate outside the injection interval, where it consists only of independent activity.

Let us first consider the case of homogeneously inserted coincidences. Trivially, the larger the analysis window T_w, the more coincidences are expected and detected. In the case of two parallel neurons, we expect $n_{exp} = (\lambda \cdot h)^2 \cdot \frac{T_w}{h}$, while observing $n_{emp} = \lambda_c \cdot T_w + (\lambda_b \cdot h)^2 \cdot \frac{T_w}{h}$ coincidences. The larger the coincidence rate, the larger the increase in detected empirical coincidences with increasing T_w (Fig. 10.4A, top, black curves). The expected number of coincidences also increases with T_w (horizontal axis, bottom panel), however, in the same way for all λ_c (Fig. 10.4A, top, dashed curve). The graphs in the bottom panel show the corresponding surprise values as functions of the size of T_w for the different injection rates. Note that for a larger coincidence rate λ_c, the significance level of 1% (dashed line in bottom panels) is reached at a smaller T_w. The values chosen for the coincidence rate were taken in the range detected in experimental data (Grün et al. 1999; Denker et al. in press), i.e., in the range of a few Hz. We find that a minimal size of the analysis window T_{min} is required for detecting excess coincidences as significant. If the analysis window is chosen smaller, the difference of n_{emp} and n_{exp} is too small to be detected as significant. On the other hand, the required difference is not a constant value but scales with the expected number of coincidences: the larger n_{exp}, the more excess coincidences are required, as is indicated by the minimal number of coincidences required for significance n_α (Fig. 10.4A, top, gray). Note that n_α increases in discrete fashion due to the discrete nature of the Poisson distribution, thereby also reflecting changes of the effective significance level (see also Pauluis and Baker 2000).

In case the time interval containing excess coincidences is limited ("hot region"), additional constraints on the detectability of excess synchrony are imposed. Consider a hot region of duration T_c (gray bar in Fig. 10.4B, bottom) and an analysis window of width T_w centered on T_c. For increasing T_w, the empirical count increases linearly up to $T_w = T_c$ due to the increasing amount of injected coincidences. As described for the homogeneous case above, depending on the injected

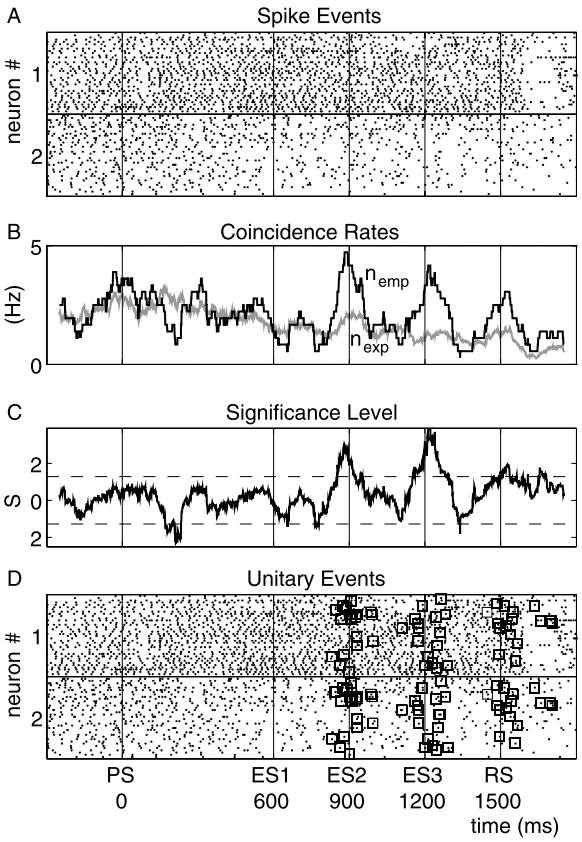

Fig. 10.3 Temporal modulation of synchronous activity. UE analysis of two simultaneously recorded single neurons from motor cortex of awake behaving monkey. The monkey was involved in a delayed pointing task, where the duration of the preparation period (after the preparatory signal (PS) up to the reaction signal (RS)) for the movement was selected randomly from four possible durations (PP; 600, 900, 1200, 1500 ms) from trial to trial. The 36 trials with longest PP duration (1500 ms) were pooled in this example. Thus the monkey could expect the RS to occur at three successive moments (ES1, ES2, ES3) before it actually occurred at RS. **A**. Raster displays of spike discharges of two neurons. **B**. Comparison of measured (*black*) and expected (*gray*) coincidence rates. Allowed coincidence width ± 2 ms. **C**. Surprise as a function of trial time. **D**. Dot display with Unitary Events (*squares*) detected based on a significance level of $\alpha = 0.05$, in sliding windows of $T_w = 100$ ms. (Modified from Riehle et al. 1997.)

coincidence rate, n_{emp} may become significant at a minimal analysis window size T_{min}. A further increase of T_w beyond T_c only leads to an accumulation of chance coincidences from outside the hot region; therefore, the slope of n_{emp} is reduced to the slope of n_{exp}, only maintaining the offset. As a consequence, the distance to the minimal number of coincidences necessary to reach the significance threshold (n_α) shrinks, and the surprise decreases until it falls below the significance level at T_{max}. Thus, the detection of injected coincidences requires $T_{min} < T_w < T_{max}$. The

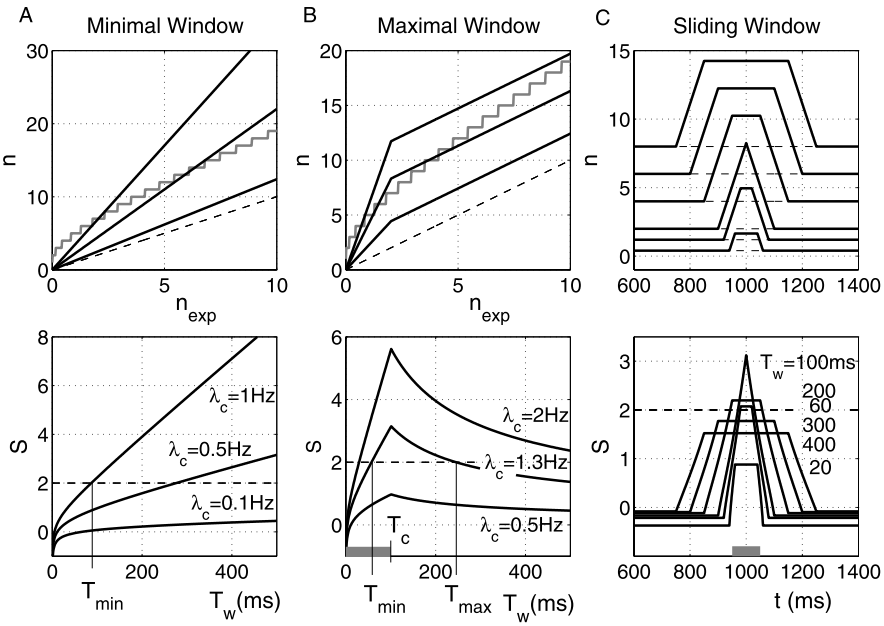

Fig. 10.4 Impact of analysis window size. All *subfigures* show in the *top panels* the coincidence count, and in the *bottom panels* the corresponding surprise value. Two parallel neurons are considered, both of a total firing rate of $\lambda = 20$ Hz, in $M = 50$ trials, significance level is $\alpha = 0.01$ corresponding to $S_\alpha = 2$ (*dashed lines* in *bottom panels*). The background rate during a coincidence injection is $\lambda_b = \lambda - \lambda_c$. **A**.–**B**.: Measures as functions of the analysis window width T_w (*horizontal axis* in *bottom panel*) that can also be interpreted as functions of n_{exp} (*horizontal axis top panels*) for given parameters. n_α as a function of n_{exp} is shown in *gray*, and the diagonal $n(T_w) = n_{exp}(T_w)$ as *dashed*. **A**. Homogeneously injected coincident events. Three curves of n_{emp} as functions of T_w for $\lambda_c = 0.1$, 0.5, 1.0 Hz (*top*) and the corresponding surprise curves (*bottom*). The crossings of n_{emp} with n_α indicate T_{min} (marked for $\lambda_c = 1.0$ Hz) values for the different coincidence rates, or correspondingly the crossings of S with the significance threshold S_α for $\alpha = 0.01$ (*dashed*, *bottom*). **B**. Injected coincidences within a hot region. Curves for injection rates $\lambda_c = 0.5$, 1.3, 2.0 Hz are shown for increasing T_w centered at the hot region ($T_c = 100$ ms, *gray bar*). The crossings of n_{emp} with n_α (or correspondingly S (*bottom*) with S_α (*dashed*)) before the bend in slope indicate T_{min} (marked for $\lambda_c = 1.3$ Hz), the crossings after the bend indicate T_{max} (marked for $\lambda_c = 1.3$ Hz). **C**. Time-resolved sliding window analysis. A hot region of width $T_c = 100$ ms (*gray bar*) with fixed $\lambda_c = 1.3$ Hz is centered at 1000 ms. $n_{emp}(t)$ and $S(t)$ are shown for different analysis window widths (from *bottom* to *top*: $T_w = 20$, 60, 100, 200, 300, 400 ms). The corresponding expected number of coincidences are constant throughout the trial (*dashed lines*)

larger λ_c, the larger T_{max} and the smaller T_{min}, and, consequently, the larger the range of possible T_w in which excess coincidences are detected as significant. For any $\lambda_c > 0$, the surprise peaks at $T_w = T_c$, even for nonsignificant outcomes, i.e., $T_{min} > T_c$.

Figure 10.4C illustrates the situation for an analysis window sliding along the data. The three measures n_{emp}, n_{exp}, and surprise S resulting from the analysis are indicated at the center position of the respective analysis window. The top panel

shows $n_{\mathrm{emp}}(t)$ for different analysis window widths ($T_{\mathrm{w}} = 400$, 300, 200, 100, 60, 20 ms, top to bottom curves). The corresponding $n_{\mathrm{exp}}(t)$ curves (dashed) are stationary but have a different offset depending on T_{w}. The empirical coincidence count starts to increase when the sliding window reaches the hot region (gray bar), assumes a peak value or plateau, and decays again when the window leaves the hot region. The larger T_{w}, the larger the maximum value of $n_{\mathrm{emp}}(t)$. However, as discussed above, significance does not depend on the absolute number of empirical coincidences but on its amount relative to the expected number, which increases for larger T_{w}. Thus, for the example values of T_{w} shown in Fig. 10.4C, only a few curves become significant, i.e., in the cases where $T_{\mathrm{min}} < T_{\mathrm{w}} < T_{\mathrm{max}}$, which for $T_{\mathrm{c}} = 100$ ms is fulfilled at $T_{\mathrm{w}} = 200$, 100, 60 ms. The shape of the surprise curve only depends on the size of T_{w} relative to T_{c}: for $T_{\mathrm{w}} \leq T_{\mathrm{c}}$, the plateau is as large as T_{c}, then becomes narrower with increasing T_{w}, until it exhibits a cusp at $T_{\mathrm{w}} = T_{\mathrm{c}}$. This process is accompanied by an increase in the maximum surprise value. For $T_{\mathrm{w}} > T_{\mathrm{c}}$, the plateau broadens at the cost of a declining amplitude.

In practice we do not know the width of any hot region in the data beforehand. We therefore suggest to vary the analysis window and observe the shape and height of the joint-surprise curve: at a triangular shape, the width of the window corresponds to the duration of the period of excess synchrony, and the analysis is adjusted to maximum sensitivity.

10.3.2 Firing Rate

Next, we study the detection reliability of UEs as a function of the firing rate of the neurons and the injected coincidence rate. We choose λ_{c} in the range of a few Hz as found in experimental data (Grün et al. 1999; Denker et al. in press). The total rate of the neurons is varied between $\lambda = 1, \ldots, 100$ Hz. Figure 10.5A shows the detection rate (true positives) of the coincidence pattern with the largest possible number of spikes ("complexity" $\xi = N$) for systems with different numbers of neurons N. The curves of a particular color correspond to specific total number of neurons ($N = 2, \ldots, 5$) at four different injection rates ($\lambda_{\mathrm{c}} = 0, 1, 2, 3$ Hz). The lower the number of neurons and the lower the injected coincidence rate, the earlier detectability is corrupted by increasing background rate. The reason is that the relative amount of excess synchrony compared to the predicted level is decreasing with increasing firing rate, leading to a nonlinear decrease in the surprise value (compare Fig. 10.4A). For systems of more neurons but the same coincidence rate, this decay is slower because the expected number of occurrences of a synchronous pattern drops with increasing complexity ξ like

$$n_{\mathrm{exp},\xi} = \frac{T_{\mathrm{w}}}{h} \cdot M \cdot P_{\mathrm{exp},\xi} = \frac{T_{\mathrm{w}}}{h} \cdot M \cdot p^{\xi} \cdot (1-p)^{N-\xi}. \tag{10.5}$$

Thus, for an $N = 5$-neuron system, coincidences of $\xi = 5$ injected at a rate of $\lambda = 3$ Hz are perfectly detected even at high firing rates (Fig. 10.5A, red curve with diamonds), whereas pair coincidences are down to a detection rate of about 50% at a background rate of about 50 Hz.

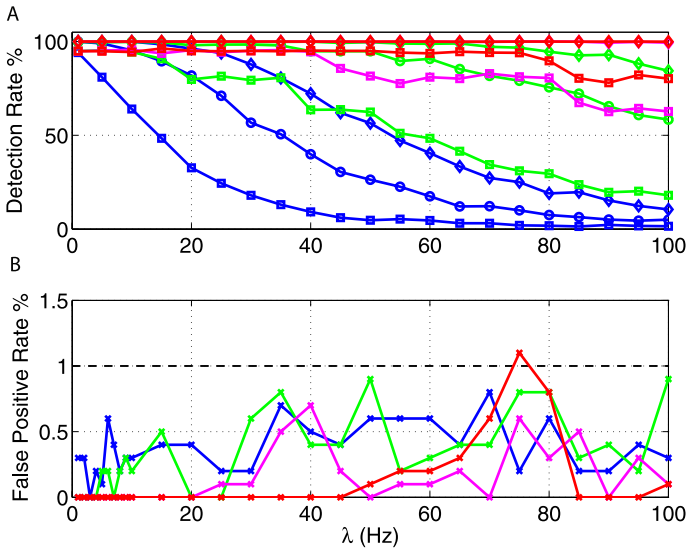

Fig. 10.5 True positive and false positive rates as functions of firing rate for systems with different numbers of neurons. Each data point is the result of 1,000 Bernoulli process realizations of N parallel neurons at stationary rate (*horizontal axis*, varied from 1 to 100 Hz), with injected coincidences (**A**. $\lambda_c = 1, 2, 3$ Hz) and without (**B**. $\lambda_c = 0$ Hz), of total duration $T = 3$ s (corresponding e.g. to $M = 30$ trials and $T_w = 100$ ms). The background rate is $\lambda_b = \lambda - \lambda_c$. The range of firing rates corresponds to spike counts of a single neuron ranging from a mean of 3 to 300. Each realization is evaluated for its empirical n_{emp} and expected n_{exp} coincidence count, and its significance ($\alpha = 0.01$). The number of neurons in the evaluated system is varied from $N = 2, \ldots, 5$ indicated by *blue*, *green*, *magenta*, and *red*, respectively. For each N, the statistics is shown for the spike coincidences of the largest complexity ($\xi = N$)

The false positive rate, i.e., the rate of significant outcomes in independent data (without injected coincidences) is around 1% as expected by a significance level of $\alpha = 1\%$ (Fig. 10.5B). The variation of the false positive levels, which are typically lower than the significance level of 1%, corresponds to the changes in the effective significance levels described by Roy et al. (2000). Due to the discreteness of the coincidence counts, in particular for low expected values, the effective significance level may be much lower than the prescribed α, and the significance tests are more conservative. As a result, for the experimentally realistic range of parameters studied here, we find a low false positive rate independent of the number of neurons considered.

10.3.3 Temporal Precision of Joint-Spike Events

One way to capture potential jitter in coincident spike events is to adjust the bin width accordingly. The choice of the bin width w (in units of time steps h) for detecting coincidences is optimal if the width just catches the temporal jitter of the

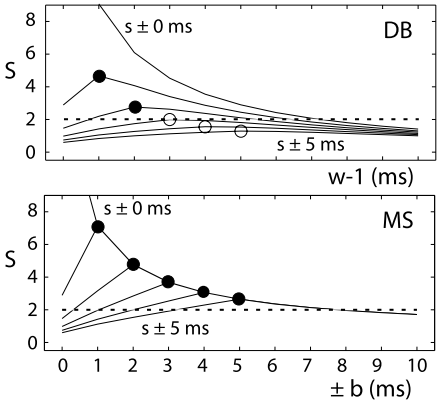

Fig. 10.6 Detection of temporally jittered coincidences. **A**. Comparison of the disjunct binning method (DB, *top*) and the multiple-shift method (MS, *bottom*) using analytical descriptions. The parallel spike trains are assumed as stationary Poisson processes ($\lambda_1 = \lambda_2 = 30$ Hz) with inserted coincident events ($\lambda_c = 1$ Hz) of a given temporal jitter ($s = \pm 0, 1, \ldots, 5$ ms, different curves). The graphs show the surprise for increasing analysis widths (*top*: for bin sizes w ranging from 1 to 11 ms; *bottom*: for maximal shifts from $b = \pm 0, \ldots, \pm 10$ ms; both in steps of $h = 1$ ms). For better visualization, the *horizontal axes* are aligned to correspond to the same maximal spike distances ($b = w - 1$). Each of the *surprise curves* shows a distinct peak, marked by *filled circles* if the values are above the significance level of $\alpha = 0.01$, i.e., $S = 2$, and marked by an *empty circle* if below. The values of S for $b = w - 1 = 0$ (not shown) are 16.76 (DB) and 16.73 (MS). (Modified from Grün et al. 1999.)

coincidences. Of course, also this width is not known in advance, but predictions may be available based on results from other analyses or on the biophysical properties of the neuronal system under study. One way of optimally adjusting the bin width is to systematically vary w. Using simulated data, generated by the injection of coincident events in otherwise independent data, one can show that the significance is largest at the optimal bin width (Fig. 10.6A) (Grün et al. 1999). The peak in the surprise S can be understood as follows: Up to the optimal bin width, more and more of the existing coincidences are detected. At the optimal width, the maximal number is reached. For larger allowed coincidence widths, the number of coincidences only increases because of chance coincidences thereby reducing the relative contribution of excess coincidences and, consequently, significance.

However, binning has a considerable drawback; there is a high probability that coincidences are split by the bin borders such that contributing spikes fall into neighboring bins and, thus, are not detected as coincidences. The division of the time axis into disjunct bins (DB) can lead to a considerable loss of the originally existing coincidences of up to 60% for bin sizes equal to the temporal jitter of the coincidences (Grün et al. 1999). One way to avoid this is to leave the data on a rather fine temporal resolution and shift the spike trains against each other up to the allowed coincidence width b (multiple-shift method (MS), Grün et al. 1999). In this case, the analytical expression for the expected number of coincidences needs to be adjusted to account for the various shifts l. For two parallel spike trains $i = 1, 2$ and M trials, this yields:

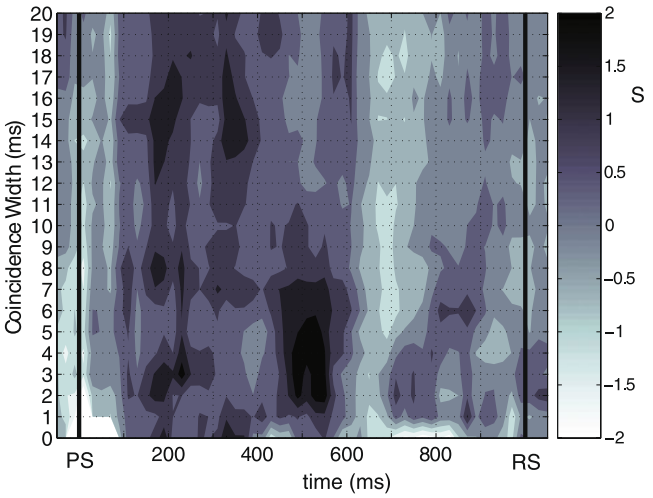

Fig. 10.7 Dynamic changes in coincidence precision. Two simultaneously recorded neurons recorded from monkey motor cortex while the animal was involved in a movement preparation task (for details, see Riehle et al. 2000). PS indicates the time of the preparatory signal, and RS the response signal. The data are analyzed for UEs by the sliding window approach ($T_w = 100$ ms, offset 20 ms). To account for jittered synchronous spikes, the multiple-shift analysis is applied, with variable coincidence widths ranging from $1, \ldots, 20$ ms. The surprise function is calculated separately for each coincidence width and then displayed in matrix form (*horizontal axis*: trial time, *vertical axis*: coincidence width). The surprise values ranges from -2.19 to 2.42, displayed here in *gray scale* (see *color bar*, display clipped below -2 to *white* and above 2 to *black*). (Modified from Riehle et al. 2000.)

$$n_{\text{exp}}^{MS} = \sum_{j=1}^{M} \sum_{l=1}^{2b+1} p_{i=1,j}\, p_{i=2,j,l}\, T_w, \tag{10.6}$$

where $p_{i,j,l}$ is the firing probability of neuron i in trial j at shift l. In this calculation, the number of coincidences resulting from the various shifts is assumed to be independent, which is not necessarily the case in real data. The multiple-shift approach is more sensitive to excess coincidences, and the significance at the optimal coincidence width is considerably larger compared to disjunct binning.

By systematic variation of the maximal shift, the MS method enables us to uncover the typical temporal precision of excess synchronous events in experimental data as the coincidence width with the largest significance. Grün et al. (1999) and Pazienti et al. (2008) found, in two different cortical systems and with different analysis approaches, very similar typical coincidence widths of a few ms. A time-resolved analysis enables us to observe also the dynamics of the temporal precision of coincident events and its relation to the behavioral protocol (Fig. 10.7). In the example shown here, the spike synchrony changes during the trial not only in strength (change in surprise values) but also in temporal precision (Riehle et al. 2000). With a latency of about 200 ms, after the preparatory signal, neuronal activity becomes significantly synchronized at a low temporal precision (jitter of 15 ms). The precision

then increases to a maximum (jitter 2–4 ms) in the middle of the preparatory period at 500 ms. During the remaining time in the preparatory period, neurons become desynchronized and fire independently.

10.4 Impact of Nonstationarities and Other Violations of Assumptions

The basic Unitary Event analysis relies on assumptions, which are typically not fulfilled in experimental neuronal data. The most obvious violation is that firing rates change as functions of time (nonstationarity in time). Another type of nonstationarity is that the base level of firing may change across trials (cross-trial nonstationarity). Latency variability, i.e., variability in the onsets of the rate changes across trials (see, e.g., Richmond 2009; Nawrot et al. 2003), may be seen as a combination of the two. Furthermore, the spike train interval statistics of experimental data (e.g., shape of interval distribution Baker and Lemon 2000, spike-count variability and spike-train irregularity Nawrot et al. 2008a, serial correlations between successive intervals Nawrot et al. 2007) often indicate that the data do not follow Poisson statistics. In the following, we discuss the impact of these features on the UE analysis, in how far they can be tolerated, and how we can cope with biologically realistic properties by incorporating them into the statistical test.

10.4.1 Nonstationary Rates

In the basic UE analysis it is assumed that the firing rates of the neurons are stationary within the analysis time window T_w. If rates change as functions of time, the average rate is not a good description of the rate profile. As a consequence, the expected number of coincidences may not be correct and could give rise to false positive outcomes. The most intuitive way to treat such cases would be to cut the data into stationary pieces and perform the analysis separately in each of those. However, this requires to find time segments that are jointly stationary for all the neurons under consideration. This, in turn, first requires reliable rate estimation and, second, detection of joint-stationary regions (see Appendix D in Grün et al. 2002b). While the idea is appealing, it heavily depends on reliable rate estimation, which is not a trivial task, in particular, if the rate is to be estimated in single trials (e.g., Nawrot et al. 1999; Ventura et al. 2002; Shimazaki and Shinomoto 2010 and Chap. 2 by Shimomoto). In addition, temporal segments corresponding to the joint-stationary regions need to be analyzed independently from each other, and, thus, a smooth transition in time is not given. For these reasons, this route has not been further explored.

An alternative idea is to slide a window of predefined width along the data and carry out the UE analysis separately in each of the windows (Grün et al. 2002b) as introduced in Sect. 10.2.4 to capture the potential dynamics of synchrony. Within

the window, data are assumed to be stationary. We now address the question which consequences we have to expect in terms of false positives (FP) if the rates are not stationary within the analysis window and how much nonstationarity can be tolerated before leading to FPs. For doing this, we consider the worst-case scenario: (1) neurons change their rates in a step-like fashion, and (2) neurons change their rates simultaneously.

For simplicity, we consider here the situation of two neurons changing their rate at the same time from λ_1 to λ_2. The duration of the interval of rate λ_1 is $t_1 = f \cdot T_\mathrm{w}$, and the duration of the second interval of rate λ_2 is $t_2 = T_\mathrm{w} - f \cdot T_\mathrm{w} = (1-f) \cdot T_\mathrm{w}$. We assume that this holds for all trials M. Ignoring the rate change implies to calculate the expected number of coincidences based on the average rate $\bar{\lambda} = \lambda_1 \cdot f + \lambda_2 \cdot (1-f)$ within T_w:

$$\tilde{n} = \bar{\lambda}^2 h^2 \cdot T_\mathrm{w} \cdot M = \big(\lambda_1 \cdot f + \lambda_2 \cdot (1-f)\big)^2 h^2 \cdot T_\mathrm{w} \cdot M. \tag{10.7}$$

However, the correct number of expected coincidences is obtained by calculating the expected number of coincidences separately for each of the stationary rate periods and then taking the sum of the two:

$$n_* = n_{*,1} + n_{*,2} = (\lambda_1 \cdot h)^2 f T_\mathrm{w} M + (\lambda_2 \cdot h)^2 (1-f) T_\mathrm{w} M. \tag{10.8}$$

Note that summation and multiplication are exchanged in the two expressions. Thus, for $\lambda_1 \neq \lambda_2$, n_* is larger than $\tilde{n}$, since the latter underestimates the expected number of coincidences. As a consequence, we tend to overestimate the significance of the empirically found coincidences n_* and obtain false positives. The amount of FPs for a given rate difference can be computed as the part of the area of the coincidence distribution with mean n_* above the minimal coincidence count n_α required for significance derived on the basis of the coincidence distribution with mean $\tilde{n}$:

$$FP = \sum_{n=n_\alpha}^{\infty} \frac{(n_*)^n}{n!} \cdot \exp(-n_*) \tag{10.9}$$

(see Grün et al. 2003 for details and Fig. 5 therein for illustration). Figure 10.8A shows the FP percentage as a function of the rate difference $\Delta\lambda = \lambda_2 - \lambda_1$ for a fixed λ_1. For increasing $\Delta\lambda$, FPs increase and at $\Delta\lambda_\alpha$ surpass the significance level $\alpha = 0.01$. Each curve (color coded) shows this dependence for a different relation f of rate level durations. The curves are nonmonotonic due to changes in the effective significance level (cf. Sect. 10.3.1).

Figure 10.8B shows the minimal rate level difference $\Delta\lambda_\alpha$ leading to FPs as functions of f for different λ_1 (color coded). For small and large f, quite large rate level differences are tolerated before FPs are induced. For intermediate values of f, the tolerated rate level difference decreases, and $\Delta\lambda_\alpha$ exhibits a minimum around $f \approx 0.6$–0.7. The exact minimum is difficult to derive due to the discretized sampling and the nonmonotonicity of FP($\Delta\lambda$). The curves for different λ_1 are similar in shape but have a systematically higher minimum for larger λ_1. For larger number of trials (or, equivalently, longer time window), the tolerated rate difference is lower, e.g., for $M = 100$, $\Delta\lambda_\alpha$ is about half as compared to $M = 30$ (not shown here).

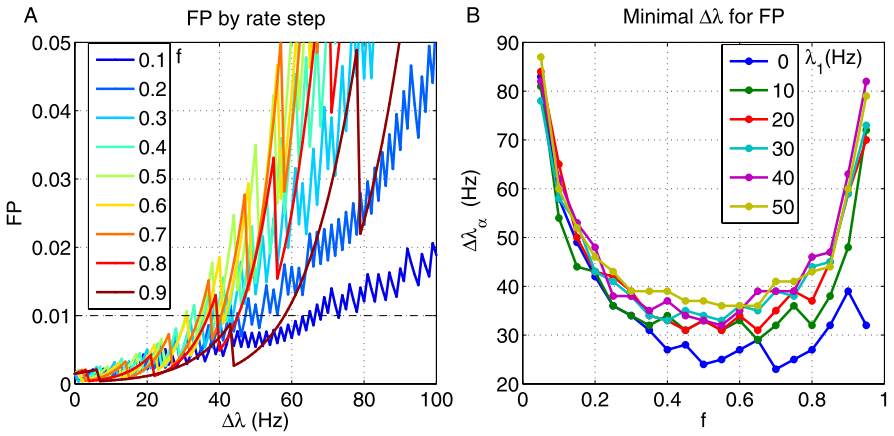

Fig. 10.8 Probability of false positives generated by coherent stepwise rate change. Two neurons are considered which change their rates stepwise in parallel from rate level λ_1 to λ_2. The relative durations of the two rate levels within the time window (here $T_w = 100$ ms) are parameterized by f. The number of trials is $M = 30$. **A**. Percentage of FPs as a function of rate difference $\Delta\lambda = \lambda_2 - \lambda_1$. λ_1 is fixed at 20 Hz, and λ_2 is varied from 20 to 120 Hz in steps of 1 Hz. Each curve is parameterized by f (color coded, see legend). The *dashed black line* shows the significance level of $\alpha = 0.01$. **B**. Critical rate relation $\Delta\lambda_\alpha$ that leads to false positives $\geq \alpha$ as a function of f (here varied in steps of 0.05 in the range $0.05, \ldots, 0.95$). Each curve is retrieved for a different λ_1. The curve for $\lambda_1 = 20$ Hz corresponds to the data shown in **A**

For the analysis of experimental data, these results imply that UE analysis shows a certain robustness to nonstationarity of rate, even if the rates change coherently and in stepwise fashion. The lower the rate level, the smaller the tolerated rate difference. In experimental data, however, rates typically do not perform such instantaneous rate jumps but rather change with finite rise times, reducing the risk of false positives even further.

10.4.2 Cross-Trial Nonstationarity

Next to nonstationarity of firing rate in time, experimental data may also exhibit nonstationarity across trials. For instance, in the simplest case, the offset of the firing rate profile may be different from trial to trial. This may be a consequence of a variation in the depth of the anesthesia or a change in the attention of the animal, etc. In analyses that involve the evaluation of first moments only (e.g., the trial-averaged firing rate), this aspect is often neglected. However, for analysis approaches that involve higher-order statistical moments, as in correlation analysis, ignorance of such cross-trial nonstationarity may lead to false positive results (Brody 1999a, 1999b; Ben-Shaul et al. 2001; Grün et al. 2003; Pauluis and Baker 2000; Ventura et al. 2005).

Here we study false positive outcomes in UE analysis if cross-trial nonstationarity of firing rates is neglected in the calculation of the predictor (Grün et al. 2003).

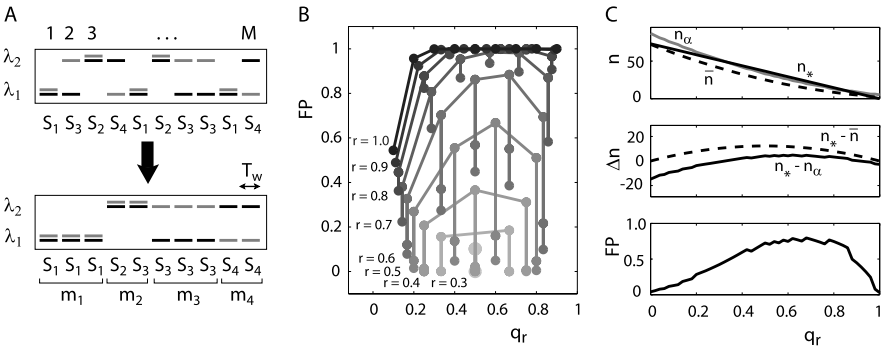

Fig. 10.9 Effect of cross-trial nonstationarity on occurrence of false positives. **A**. Example of an individual M-trial sequence and composition of rate states s_1, s_2, s_3, s_4. *Gray* refers to the rate level of neuron 1, *black* to neuron 2. Below is the reordered sequence of rate states, with $m_1 + m_2$ states forming a coherent rate step, and the remaining $m_3 + m_4$ form opposing rates. **B**. False positives *FP* as a function of rate step duration r and rate step proportion q_r (*horizontal*) for all macrostates of an example system ($\Delta\lambda = 70$ Hz, $q = 0.5$, $M = 10$, $T_w = 1000$ ms, $\alpha = 0.05$). Curves connect data (*dots*) for macrostates with identical r (as labeled, *dark gray* encodes large r, *large dots* for $r = 0.2$). Multiple values of FP at identical (r, q_r) reflect macrostates distinguished by m_3 and m_4 (*vertically connected dots*). **C**. Analysis of a coherent rate step corresponding to $r = 1$, $M = 10$, $T_w = 1000$ ms, $\alpha = 0.05$. The *upper graph* shows n_* (*black solid*), $\bar{n}$ (*dashed*), and n_α (*gray*) as functions of q_r. The *middle graph* shows the difference of the correct expected number n_* to the expected number derived by averages $\bar{n}$ (*dashed*) and to the minimal number at threshold n_α (*solid*). The *lower graph* shows the false positives FP for each pair n_* and $\bar{n}$ as a function of q_r. Steps are due to the discrete nature of n_α. (Modified from Grün et al. 2003.)

For simplicity, we again assume a system of two neurons, however, with stationary firing rates within the analysis window but with rate levels changing from trial to trial. Based on a two-rate-state model, rates are randomly drawn from two possible rate levels λ_1 (low rate) and λ_2 (high rate), independently for each trial and each neuron. Their distance $\Delta_{CT} = \lambda_1 - \lambda_2$ gives a measure for the degree of cross-trial nonstationarity. An additional parameter of the model is the probability to select one of the two rate levels ("occupation probability") termed q for λ_1 and $(1 - q)$ for λ_2. Thus, the degree of nonstationarity across trials and the occupation probability of the rate levels can systematically be varied.

One realization of M trials is composed of a sequence of four possible rate combinations ("rate states"), $[\lambda_1, \lambda_1]$ called s_1, $[\lambda_2, \lambda_2]$ called s_2, $[\lambda_1, \lambda_2]$ called s_3, and $[\lambda_2, \lambda_1]$ called s_4 (Fig. 10.9A, top panel). The occurrence counts of the respective rate states $[m_1, m_2, m_3, m_4]$ depend on the occupation probabilities of the rate levels defined by q (see derivations in Grün et al. 2003). As in the foregoing section, we are interested in the FP probability originating if nonstationarity is ignored. The number of coincidences expected under the assumption that rates are identical across trials is given by the rate averages $\bar{\lambda}_1$ and $\bar{\lambda}_2$ across trials:

$$\bar{n} = \bar{\lambda}_1 h \cdot \bar{\lambda}_2 h \cdot T_w \cdot M = \left(\frac{1}{M}\sum_{i=1}^{M} \lambda_{1,i}\right) h \cdot \left(\frac{1}{M}\sum_{i=1}^{M} \lambda_{2,i}\right) h \cdot T_w \cdot M. \qquad (10.10)$$

The correct expected number of coincidences is the sum of the expected number of coincidences per trial $n_{*,i}$:

$$n_* = \sum_{i=1}^{M} n_{*,i} = \left(\sum_{i=1}^{M} \lambda_{1,i} h \cdot \lambda_{2,i} h \right) \cdot T_{\mathrm{w}}. \tag{10.11}$$

Note, as in the foregoing section, the interchange of sum and product in the two expressions. With these two expressions, we are able to calculate the FP rate as above by calculating the area of the Poisson coincidence distribution with mean n_* starting at $\bar{n}_\alpha$ derived from the coincidence distribution with mean $\bar{n}$ (cf. (10.9)). However, the number of possible rate state realizations across M trials ("microstates") is huge because the four possible rate states s_i may occur in different sequences and numbers of occurrences m_i. Fortunately, the expressions for the number of coincidences are not dependent on the specific sequence of the rate states, but just on their nature. Therefore, we can reduce the complexity by combining all microstates with the same number of rate state occurrences $[m_1, m_2, m_3, m_4]$ into one macrostate. The coincidence counts of a macrostate are then calculated as

$$\bar{n}_m = \left(\frac{1}{M} \sum_{i=1}^{4} m_i \lambda_{1,i} h \right) \cdot \left(\frac{1}{M} \sum_{i=1}^{4} m_i \lambda_{2,i} h \right) \cdot T_{\mathrm{w}} \cdot M \tag{10.12}$$

and

$$n_{*,m} = \left(\sum_{i=1}^{4} m_i \cdot \lambda_{1,i} h \cdot \lambda_{2,i} h \right) \cdot T_{\mathrm{w}}. \tag{10.13}$$

We can think of the consecutive trials $1, \ldots, M$ as a temporal sequence of time segments. By ordering the rate states as a sequence of first low–low rates (m_1 times s_1), followed by a region where both neurons have high rates (m_2 times s_2), and two regions with opposing rates (m_3 times s_3, m_4 times s_4), the temporal sequence can be viewed as a coherent rate step followed by anticorrelated rate levels (Fig. 10.9A, bottom panel). This situation is very similar to the one treated for covarying rate steps in Sect. 10.4.1, with the difference that there the rate steps lasted for the whole duration of time considered. Here, a part of the time sequence of duration $(m_3 + m_4) \cdot T_{\mathrm{w}}$ contains opposing rates (states s_3 and s_4).

We characterize a macrostate more compactly by the relative length of the rate step $r = \frac{m_1+m_2}{M}$ and the relative duration of the low-rate and high-rate regimes $q_r = \frac{m_1}{m_1+m_2}$, a relation comparable to the relation f in the foregoing. In Fig. 10.9B we use the variables r and q_r to structure the set of macrostates of a system with $M = 10$ trials in terms of false positives. Macrostates containing a rate step generate a high fraction of false positives. (The absolute FP rate is higher than in the example shown in Sect. 10.4.1, because here T_{w} is 10 times larger than in the former example.) The longer the rate step (large r), the larger the fraction of false positives. For constant r, the FPs reach a maximum at q_r close to ≤ 0.7. Figure 10.9C demonstrates the relation of the expected number of coincidences n_* and $\bar{n}$ to the minimal number required to be significant (n_α) (top panel). The numbers n_* and $\bar{n}$ decrease

in different manner with the expansion of the low-rate regime, i.e., increasing q_r. The difference of the two (middle panel) exhibits a maximum at $q_r = 0.5$. However, the false positive rate for each pair of $n_*, \bar{n}$ (bottom panel) reaches a maximum at $q_r \approx 0.7$ due to the nonlinearity involved in the calculation of the significance (cf. Fig. 10.4A).

10.4.2.1 Intermediate Summary on Nonstationarities

In conclusion, the most effective generator of false positives turns out to be covariation of firing rates across trials, i.e., trials where both neurons are in the same of the two rate states. The rate of false positives is maximal, if in approximately 70% of the trials, the neurons are jointly in the low-rate state, the remainder in the high-rate state. However, directly including the trial-by-trial spike counts and calculating the expected number of coincidences in a trial-by-trial manner (10.2) avoids the occurrence of FPs.

This consideration of cross-trial nonstationarity can also be interpreted in the context of nonstationarity in time, by reinterpreting the trials as time segments. In this view, the most efficient generator of false positives is a step of coherent firing rates, with 70% of the time spent in the low–low rate configuration, and 30% in the high–high rate configuration. The longer the duration of the coherent rate step, compared to the full duration of the data set, the more false positives are generated. In the extreme, the complete data set represents a coherent rate step as studied in Sect. 10.4.1 (see also Kass and Ventura 2006 for a related aspect). Unfortunately, there is no such simple solution for nonstationarity in time as we had for the cross-trial nonstationarity. Theoretically, the solution is straightforward if the bin-by-bin firing probabilities $p_{i,k,j}$ are known, with i being the neuron index:

$$n_{\mathrm{exp}} = \sum_{j=1}^{M} \sum_{k=1}^{T_{\mathrm{w}}/h} p_{1,k,j} \cdot p_{2,k,j}. \tag{10.14}$$

This would also be a way of calculating the expected number of coincidences for combinations of nonstationarities in time and cross-trial, even in the absence of coherent onsets of rate changes (latency variability). However, the problem is the *estimation* of the firing probabilities, which typically involves taking averages (Nawrot et al. 1999; Ventura et al. 2002; Shimazaki and Shinomoto 2010) either across trials or over time and thus is not as instantaneous as required.

A practical solution is to choose a nonparametric approach, i.e., the generation of the coincidence distribution for the significance test on the basis of surrogate data. The idea is to specifically destroy in the original data the feature one is going to test for, in our case the exact temporal coordination of spikes across neurons, but to conserve all other statistical properties of the original data (see Sect. 10.5.1 below for details). The coincidence distribution results from the different coincidence counts of a sufficiently large number of surrogate data sets.

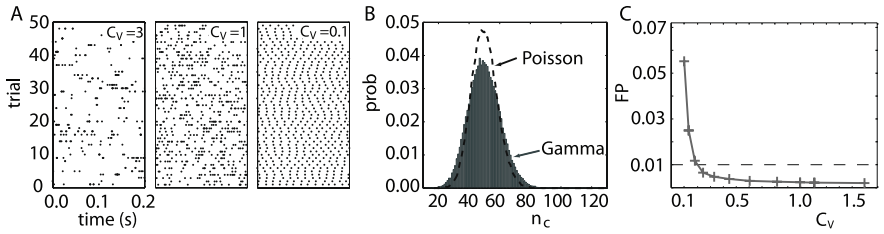

Fig. 10.10 Impact of non-Poisson spike trains on significance estimation. **A**. *Dot* displays of three different examples of realizations of Gamma processes (*left to right*: $C_V = 3$ ("bursty"); $C_V = 1$ (Poisson); $C_V = 0.1$ (regular)). **B**. Comparison of coincidence distributions of two parallel spike trains (*dashed*: Poisson; *gray*: Gamma process with $C_V = 0.1$; firing rates are 50 Hz, $M = 10^5$ trials of 5-s duration, bin width $h = 4$ ms, no clipping). **C**. Coincidences are evaluated based on binning ($h = 4$ ms, clipped). Both processes are parameterized by the product of bin width and firing rate, here 0.1. Probability of false positives (UE analysis, Poisson assumption; significance level $\alpha = 0.01$) for coincidences detected in pairs of independent Gamma processes (rates $\lambda = 50$ Hz, 10^4 realizations of 5 s for each C_V). (Modified from Grün 2009.)

10.4.3 Non-Poisson Processes

The UE analysis method as presented so far assumes the individual spike trains to have Poisson statistics. However, neuronal spike trains often deviate from this assumption. This poses the question to what extent UE analysis is affected by the properties of the individual processes. In particular, whether an error in the assumed process type (here: Poisson) influences the significance estimation of spike coincidences. To investigate this, we model spike trains as renewal processes with interspike intervals (ISIs) drawn from a Gamma distribution (see, e.g., Chap. 16 by Cardanobile and Rotter), which is presently considered to be a reasonable model for experimental spike trains (see references in Nawrot et al. 2008a).

Figure 10.10A shows dot displays of example realizations of a Gamma process for three parameter settings. The processes are parameterized by their coefficient of variation $C_V = \frac{\sigma(ISI)}{\mu(ISI)}$. Processes with higher ISI variability than Poisson ($C_V = 1$) have a C_V larger than 1, and processes with more regular ISIs than Poisson have values smaller than 1 (see Chap. 3 by Nawrot). Figure 10.10B illustrates the distribution of coincidence counts derived from simulations of parallel, stationary, and independent Gamma processes. The shape of the coincidence distribution changes with C_V (or, correspondingly, with the shape of the ISI distribution). For the investigated process type, the distribution is unimodal and becomes wider for $C_V > 1$. For $C_V < 1$, the distribution first gets narrower than Poisson and for even smaller C_V widens again. For unclipped processes (i.e., bins may contain more than 1 spike), the mean of the distribution is the same as for the Poisson process, fully defined by the firing rates of the neurons (Pipa et al. under revision).

Yet, in spite of these obvious deviations from the simple Poisson assumption, UE analysis is in large parts unaffected if the spike trains have Gamma-renewal statistics. Only for very regular processes ($C_V \ll 1$), UE analysis leads to an increased number of false positives. Nevertheless, the significance of coincident events of pro-

cesses with moderate $C_V < 1$ or bursty processes ($C_V > 1$) tends to be underestimated (Fig. 10.10C). The reason why UE analysis does not generate false positives for bursty processes is twofold. First, it operates on binned and clipped spike trains, which considerably reduces the burstiness and leads to a Poisson-like coincidence distribution. Second, UE analysis adjusts the mean of the distribution used for the significance evaluation according to the spike counts in the data under evaluation (Pipa et al. in preparation). Most cortical data show a $C_V > 0.2$ (Nawrot et al. 2008a) leading to the conclusion that when Poisson processes are wrongly assumed, the test is more conservative and does not generate FPs, as was also found in Pipa et al. (2007). A further study extending the scope to nonrenewal processes with first-order negative serial correlation, as found in cortical data (Nawrot et al. 2008a), shows the same general findings (Nawrot et al. 2008b).

Taken together, these results show that the temporal structure of the spike trains influences the significance evaluation of coincident spike events. If Poisson statistics are assumed, the significance may be under- or overestimated, depending on the C_V of the analyzed processes. Obviously, it is preferable to use the proper coincidence distribution for the significance test. Unfortunately, to the best of our knowledge, there is currently no analytical expression for the coincidence distribution, given the C_V, available.

One solution would be to model the simultaneous processes as independent processes and to generate the coincidence distribution from simulated data. However, this requires knowledge about the statistics of the measured data for proper model selection. This is not a trivial task, since ISI distributions of experimental data are often confounded by changes of the firing rates (Baker and Lemon 2000; Johnson 1996). This problem may be solved by time-rescaling approaches, making the firing stationary prior to constructing the ISI distribution and performing parameter estimation (Nawrot et al. 1999, 2008a; Brown et al. 2002). This procedure relies on the assumption that the process parameters do not change in time. If they do, parameters have to be estimated in a time-dependent manner. Another way to create the proper distribution without having to assume a certain point process model is to generate the distribution directly from the measured data with the help of surrogate data (Pipa et al. 2007, 2008; Ito 2007; Louis et al. in press, see Sect. 10.5.1).

10.5 Discussion

Unitary Event analysis is a tool for the analysis of time-dependent spike correlations. Its application has provided important insights into principles of information processing in the cortex in a number of studies. In the visual (Maldonado et al. 2008), the prefrontal (Grün et al. 2002b), and the motor cortex (Riehle et al. 1997, 2000; Grammont and Riehle 1999, 2003; Kilavik et al. 2009), Unitary Events occur at distinct and relevant points in time during the behavior, which could not have been detected by conventional cross-correlation analysis due to averaging over time. Changes in firing rates and spike synchrony often occur in complementary fashion

and may even show complementary tuning. The precision of UEs is typically found in the range of a few ms (Grün et al. 1999) but may also change as a function of time during the trial.

The existence and functional role of spike synchrony are still debated, although both theoretical (Abeles 1982; Bernander et al. 1994; Diesmann et al. 1999; Goedeke and Diesmann 2008; Marsalek et al. 1997; Kumar et al. 2008) and experimental (e.g., Reyes 2003; Rodriguez-Molina et al. 2007) studies have shown that neurons are much more likely to exhibit output spikes if the input activity is synchronized. Reliable tools to decide between rate fluctuations and spike synchrony are required. In this chapter we have outlined the properties and assumptions of UE analysis and have also demonstrated the limitations of the analysis based on analytical expressions for the expected number, the coincidence distribution, and, thus, the significance of coincident events. As we showed, UE analysis can tolerate a reasonable range of nonstationarities and deviations from Poisson before causing false positives. Still, to avoid a wrong interpretation of experimental data, we suggest the following approach: Start the analysis of the data with the UE analysis based on the null hypothesis expressed by (10.2). If there are UEs at time instances were firing rates change abruptly, or the spike trains are extremely regular, perform additional tests by intentionally destroying spike coincidences, or by modeling neuronal activity (Maldonado et al. 2008; Pazienti et al. 2008), or by comparing the analysis results with the results of other analyses (e.g., as done in Pipa et al. 2007), or directly apply nonparametric tests based on surrogates (see below). We stress that these concerns are not specific to UE analysis but apply to any correlation analysis method since any method has specific assumptions that may be violated by the data (Grün 2009).

In the following, we will discuss three further issues of interest in connection to UE analysis. First, we discuss the use of surrogate data as an alternative approach in the analysis of significance. Second, we discuss the use of UE analysis as a time-dependent measure of synchronization in population activity. Finally, we briefly describe the relation between UE analysis and other correlation-based methods of neuronal ensemble activity.

10.5.1 Surrogates

UE analysis rests on a number of assumptions, like stationarity of the processes within the analysis time window and Poisson statistics of the individual processes involved. Under these conditions, the analysis can be performed computationally fast since the distribution for the statistical test (Poisson distribution) is known analytically. Also the parameter for the distribution, the expected number of coincidences, can be derived from the experimental data by simply taking into account the spike counts of the neurons. Nonstationarity across trials can be directly and easily incorporated into that measure by considering the spike counts of each neuron in each trial.

Although UE analysis based on Poisson-distributed coincidence counts exhibits a certain robustness to violations of the assumptions, it is desirable to have a method to construct a coincidence distribution by taking into account more details of the experimental data. The potential advantage is not only an increased reliability (reduction of false positives, FPs) but also an increased sensitivity (reduction of false negatives, FNs). The price is an increased computation time.

One approach is to model the simultaneous processes as independent processes and to realize the coincidence distribution on this basis. This, however, also requires precise knowledge about the statistics of the measured data and reliable methods of model selection. Therefore we suggest to make use of surrogate data to directly generate the proper distribution for the significance test. Surrogate data are artificial data that are generated from the original data by specific manipulations. The idea is to specifically destroy the feature one is going to test for, while conserving all other properties of the original data. In our case the property of interest is the exact temporal coordination of the spikes across the neurons. Thus we intend to destroy the exact timing of spikes. Meanwhile there is a large body of surrogate generation methods available, each with somewhat different characteristics. Some are designed to preserve the ISI distribution of the spike trains, and others preserve the spike counts or rates but at the same time often ignore other features and destroy these. Thus, one has to carefully check the applicability of the surrogate for the question being studied. Chapter 17 by Louis et al. illustrates how to select proper surrogates for particular features present in the data (e.g., strong rate modulations, cross-trial nonstationarity, etc.) in the framework of correlation analysis. A recent review by Grün (2009) gives an overview of currently available surrogate methods, the features they preserve and those they destroy.

The way surrogates are employed for UE analysis is the following: For each position of the analysis window, we construct the coincidence distribution from surrogate data. If the significance level is specified up to two decimals, typically 1000 surrogate data sets are sufficient. Each surrogate is analyzed for the occurrence of coincidences in the same way and with the same parameters (e.g., coincidence width, number of trials) as the original data. For example, if we are interested in the significance of the spike pattern [1 0 1 1 0 0] of neurons $1, \ldots, 6$, we need to count the occurrences of the same pattern in the surrogate data. The coincidence count distribution is constructed from the different counts in the surrogates. Subsequently, the empirical count is compared to the distribution by computing the p-value or surprise. For the next sliding window position, the procedure is repeated. In practice a surrogate is typically created for the whole data set and then evaluated in sliding window fashion in order to avoid border effects.

The contribution by Louis et al. (Chap. 17) illustrates proper selection of surrogates in the context of pairwise correlation analysis of coincident spike events. The study is directly related to UE analysis, since it basically performs UE analysis between a pair of neurons for one position of the analysis window. The only difference is that in their case the analysis window spans the whole trial which includes considerable nonstationarities. Thus their results on the performances of different surrogates result from averaging across the whole trial. The study shows that proper

surrogates can well account for nonstationarities in time and across trials, and for non-Poisson ISI statistics.

Obviously, the surrogate approach is costly in computation time and memory requirements. However, with the help of today's computer clusters and high-level programming languages, this is not a practical problem. Chapter 20 by Denker et al. provides a hands-on introduction into the use of distributed and parallel computing techniques for the analysis of neuronal data.

10.5.2 Population Measures

UE analysis allows one to examine the occurrence of excess spike synchrony within a set of simultaneously recorded neurons and its relation to sensory stimulation and/or to behaviorally relevant events. For example, Riehle et al. (1997) found that neurons in monkey motor cortex synchronize their activity at instances in time when the monkey expects a go signal to initiate an arm movement, even if the signal does not occur. This leads to the interpretation that the cortical network is preparing for the upcoming movement by the activation of neuronal assemblies.

A next step is to confirm that such time- and behavior-dependent phenomena are consistent across the population of neurons. Such questions are often approached by performing many recordings of different sets of neurons from the same network, session by session, under the assumption that the recordings form representative samples. The idea is to capture phenomena reappearing consistently across the different recordings. A simple averaging of the time-dependent surprise functions (or p-value functions) across sessions is not a meaningful approach, since these measures are nonlinear and would need complicated statistical treatment in order to be averaged. An alternative is to indicate time instances that exhibit significant spike synchrony and to calculate the percentage of sessions which show excess spike synchrony at a specific instant in time. For example, if pairs of neurons are analyzed for UEs, the center bins of the sliding analysis window can be marked as "1", if the window contains excess coincidences, otherwise "0", resulting in a binary vector. Doing this for all pairs of neurons under the same behavioral condition yields binary vectors that can be averaged across the population bin-by-bin. The result is a measure of the probability of finding significant synchronization across the population at any instant in time (Riehle et al. 2000; Grammont and Riehle 2003). This time-dependent population measure can then be compared, e.g., to the firing rate averaged across the population of recorded neurons. Grammont and Riehle (2003) found by such an analysis directional tuning of spike synchrony at a specific instant in the preparatory period without any sign of rate tuning. However, the finding was reversed during movement onset which was taken as evidence that coherent activation of cell assemblies may trigger the increase in firing rate in large groups of neurons.

Kilavik et al. (2009) evaluated whether intensive practice induces long-term modifications in the temporal structure of synchrony and firing rate at the population

level. Monkeys were trained in a delayed pointing task in which the selection of movement direction depended on correct time estimation. The goal was to quantify the evolution of synchrony in time and the temporal precision at the level of the population. The observation in individual neuron pairs is that spike synchrony typically occurs in relation to an expected event, but not in a strictly time-locked fashion. Thus the approach to sum the binary vectors is not able to capture this observation. An intuitive approach would be to simply smooth the summed binary vector to allow some temporal spread of the synchrony responses. Unfortunately, the resulting values of the filtered vector cannot be interpreted as the percentage of significant pairs since they are perturbed by multiple testing. An alternative, however, is to slide an integration window along the binary vector of each pair and evaluate if the count of "1"s per window is significant compared to surrogate data. Using this approach, Kilavik et al. (2009) found that the timing of the task is represented in the temporal structure of significant spike synchronization at the population level. During practice, the temporal structure of synchrony is shaped, with synchrony becoming stronger and more localized in time during later experimental sessions, in parallel with an improvement in behavioral performance. Concurrently, the average population firing rate mainly decreases, which is interpreted as performance optimization through practice by boosting the computation via spike synchrony, allowing an overall reduction in population activity.

Another approach used in Kilavik et al. (2009) extracts the strength of the significance of spike correlation of the whole population of pairs. For a particular behavioral condition, the trial-by-trial empirical and expected numbers of coincidences are derived in each sliding window for each neuron pair. Instead of calculating the significance on a pair-by-pair basis and combining the results in terms of UE rate (Maldonado et al. 2008; Ito et al. submitted), one first sums the respective numbers of all trials and all pairs and computes the significance of the total empirical counts given the total sum of expected numbers. By performing this computation at each sliding window position, one obtains a time-dependent surprise function of the population data. All these computations are not restricted to coincidence events between pairs of neurons only but can be performed for any kind of spike pattern across multiple neurons of interest.

10.5.3 Relation to Other Analysis Methods

The standard tool of spike correlation analysis is the cross-correlation histogram (CCH; Perkel et al. 1967, Chaps. 5, 6). It analyzes spike correlation between pairs of spike trains by retrieving the probability for spike occurrence in one spike train relative to the spikes of a reference spike train. It therefore extracts delayed and near-coincidences. Normalization of the CCH by subtracting the expected number of coincidences given the firing rates and dividing by the products of the standard deviations of the spike counts provides a correlation coefficient for each time delay. The approach assumes stationarity of the firing rates and needs to integrate over

relatively long data stretches of time. A typical result of a CCH analysis is a peak around a certain delay, for cortical data typically around zero delay. However, if firing rates are nonstationary, the CCH may also exhibit a peak solely reflecting the nonstationarity of the rates and not the coordination of spike times (see illustration in Chap. 17). The fact that experimental data typically reveal synchronized or near-coincident spike events led to the focus of UE analysis on spike synchrony. Thus, UE analysis is basically evaluating the significance of coincidences with zero or small delay, which corresponds to an evaluation of the central bin entries of the CCH only. In addition, UE is performed in a sliding window manner, which can in principle also be done for the CCH but restricts the maximal delay.

The Joint Peri-Stimulus Histogram (JPSTH) analysis method provides a time-resolved spike correlation analysis (Aertsen et al. 1989). Spike coincidences of any delay of a pair of neurons are entered in a matrix with zero-delay coincident spikes along the diagonal and delayed coincidences at corresponding time delays off the diagonal. The statistics is evaluated across trials separately within each bin. Within each bin, corrections for chance coincidences are performed by computing the correlation coefficient. Along the diagonal, the tool captures the dynamics of coincidences. The applicability of the JPSTH requires a large number of trials (typically, tens to hundreds) to retrieve reliable statistics within the individual bins. In comparison, the UE analysis basically integrates the coincidence counts in a window sliding along the diagonal, thereby requiring fewer trials, but for the price of smoothed results. An approach related to the JPSTH was used for the evaluation of spatio-temporal spike patterns between three neurons (Prut et al. 1998; Abeles and Gat 2001 and Chap. 9). Here the spikes of one neuron are used as the triggers relative to which the temporal relations of the spikes of two further neurons are entered into the matrix. The matrix is actually a section of the snowflake plot (Perkel et al. 1975; Czanner et al. 2005) which was developed as a natural extension of the pairwise to a tripplewise analysis of parallel spike trains. In all these tools, except in the JPSTH, the time dependence of the patterns is lost.

As outlined in Chap. 9, the calculation of the expected number of coincidences for $N > 2$ becomes more difficult, since considerations of higher-order correlations come into play. The null hypothesis may not only be based on full independence of the firing, but should also enable us to test whether tripple events are not trivially explained by the presence of pairwise correlations. However, this makes the formulation of the null hypothesis considerably more complicated (see Chap. 12 by Staude et al.). UE analysis in its present formulation tests for deviations from full independence only. Thus a significant triplet may be the result of a significant pairwise correlation, i.e., pair coincidences coinciding with background spikes. Shimazaki et al. (2009) tackle this problem and develop a state-space-based time-resolved higher-order analysis method using the framework of information geometry (see Chap. 11 by Amari) to identify periods expressing higher-order correlations. In such an approach, the number of parameters to be estimated faces the danger of a combinatorial explosion, thereby reducing the possible number of parallel processes to be analyzed simultaneously or requires huge numbers of trials. Another approach to the analysis of synchronization in the spiking activities of larger ensembles of

neurons is given by the 'gravitational clustering' method (Gerstein et al. 1985; Gerstein and Aertsen 1985). The basic ideas of this method, later improvements, and results of its application to physiological multiple-neuron recordings are described in Chap. 8 by Gerstein.

Finally, two variants of UE analysis, each one with its specific interesting properties, should be mentioned. Gütig et al. (2002) reformulated the statistical test underlying the UE method using a coincidence count distribution based on empirical spike counts, rather than on estimated spike probabilities. This led to the hypergeometric distribution, rather than the binomial distribution, as the test distribution of interest. By analytical calculations of the test power curves of the original and the revised method, they demonstrated that the test power could be increased by a factor of two or more in physiologically realistic regimes. Moreover, in the case of two neurons, they showed that the requirement of stationary firing rates, originally imposed on both neurons, could be relaxed; only the rate of one neuron needs to be stationary, while the other may follow any arbitrary time course. A second variant, called NeuroXidence (Pipa et al. 2008), detects coincident spike events in multiple neurons by a method comparable to the multiple-shift approach and directly uses surrogate data for the generation of the null hypothesis. The method proposes a particular surrogate to use, i.e., to shift the spike trains as a whole against each other by a small amount of time to destroy spike synchrony (see also Harrison and Geman 2009 and Chap. 17). Significance of the empirical number of coincidences is evaluated by comparison with the counts resulting from the shifted versions using a t-test. A comparison of analysis results based on UE and NeuroXidence (Pipa et al. 2007) of experimental data from motor cortex of monkey confirmed the results derived using the standard UE, however with slightly higher significance. This may reflect the fact that the method is accounting for the spike train autostructure.

10.5.4 Conclusion

- The UE method provides a tool to analyze multiple parallel spike trains for time-dependent spike synchrony, enabling the study of the relation between spike synchrony and behavioral context.
- The basic UE method relies on the assumption of trial-by-trial stationary Poisson processes to enable rapid analysis on the basis of an analytical expressions for the significance estimation.
- The basic UE method tolerates reasonable amounts of nonstationarity, as well as non-Poisson ISI statistics for experimentally found C_Vs without generating false positive results.
- Concerns with respect to false positives can be alleviated by cross-checking the results using count distributions constructed from surrogate data.

The software is available at http://www.apst.spiketrain-analysis.org.

Acknowledgements Partial funding by the Helmholtz Alliance on Systems Biology, by the German Federal Ministry of Education and Research (BMBF) to DIP F1.2 and to BCCN Freiburg (01GQ0420), and by the EU-FP6 (15879, FACETS).

References

Abeles M (1982) Role of cortical neuron: integrator or coincidence detector?. Israel J Med Sci 18:83–92

Abeles M (1991) Corticonics: neural circuits of the cerebral cortex. Cambridge University Press, Cambridge

Abeles M, Gat I (2001) Detecting precise firing sequences in experimental data. J Neurosci Methods 107(1–2), 141–154

Aertsen A, Gerstein G, Habib M, Palm G (1989) Dynamics of neuronal firing correlation: modulation of "effective connectivity". J Neurophysiol 61(5), 900–917

Baker S, Lemon R (2000) Precise spatiotemporal repeating patterns in monkey primary and supplementary motor areas occur at chance levels. J Neurophysiol 84(4):1770–1780

Barlow HB (1972) Single units and sensation: a neuron doctrine for perceptual psychology?. Perception 1:371–394

Ben-Shaul Y, Bergman H, Ritov Y, Abeles M (2001) Trial to trial variability in either stimulus or action causes apparent correlation and synchrony in neuronal activity. J Neurosci Methods 111(2):99–110

Bernander Ö, Koch C, Usher M (1994) The effect of synchronized inputs at the single neuron level. Neural Comput 6:622–641

Brody CD (1999a) Correlations without synchrony. Neural Comput 11:1537–1551

Brody CD (1999b) Disambiguating different covariation types. Neural Comput 11:1527–1535

Brown E, Barbieri R, Ventura V, Kass R, Frank L (2002) The time-rescaling theorem and its application to neural spike train data analysis. Neural Comput 14:325–346

Czanner G, Grün S, Iyengar S (2005) Theory of the snowflake plot and its relations to higher-order analysis methods. Neural Comput 17(7):1456–1479

Denker M, Riehle A, Diesmann M, Grün S (in press) Estimating the contribution of assembly activity to cortical dynamics from spike and population measures. J Comput Neurosci. doi:10.1007/s10827-010-0241-8

Diesmann M, Gewaltig MO, Aertsen A (1999) Stable propagation of synchronous spiking in cortical neural networks. Nature 402(6761):529–533

Gerstein G, Aertsen A (1985) Representation of cooperative firing activity among simultaneously recorded neurons. J Neurophysiol 54:1513–1528

Gerstein G, Perkel D, Dayhoff J (1985) Cooperative firing activity in simultaneously recorded populations of neurons: detection and measurement. J Neurosci 5:881–889

Gerstein G, Bedenbaugh P, Aertsen A (1989) Neuronal assemblies. IEEE Trans Biomed Eng 36(1):4–14

Goedeke S, Diesmann M (2008) The mechanism of synchronization in feed-forward neuronal networks. New J Phys 10:015007. doi:10.1088/1367-2630/10/1/015007

Grammont F, Riehle A (1999) Precise spike synchronization in monkey motor cortex involved in preparation for movement. Experimental Brain Res 128:118–122

Grammont F, Riehle A (2003) Spike synchronization and firing rate in a population of motor cortical neurons in relation to movement direction and reaction time. Biol Cybernet 88(5):360–373

Grün S (2009) Data-driven significance estimation of precise spike correlation. J Neurophysiol 101(3):1126–1140 (invited review)

Grün S, Diesmann M, Grammont F, Riehle A, Aertsen A (1999) Detecting unitary events without discretization of time. J Neurosci Methods 94(1):67–79

Grün S, Diesmann M, Aertsen A (2002a) 'Unitary Events' in multiple single-neuron spiking activity. I. Detection and significance. Neural Comput 14(1):43–80

Grün S, Diesmann M, Aertsen A (2002b) 'Unitary Events' in multiple single-neuron spiking activity. II. Non-stationary data. Neural Comput 14(1):81–119

Grün S, Riehle A, Diesmann M (2003) Effect of cross-trial nonstationarity on joint-spike events. Biol Cybernet 88(5):335–351

Gütig R, Aertsen A, Rotter S (2002) Significance of coincident spikes: count-based versus rate-based statistics. Neural Comput 14:121–153

Harris K (2005) Neural signatures of cell assembly organization. Nature Neurosci Rev 5(6):339–407
Harrison M, Geman S (2009) A rate and history-preserving resampling algorithm for neural spike trains. Neural Comput 21(5):1244–1258
Hebb DO (1949) The organization of behavior: a neuropsychological theory. Wiley, New York
Ito H (2007) Bootstrap significance test of synchronous spike events – a case study of oscillatory spike trains. Statistical Med 26:3976–3996
Ito J, Maldonado P, Singer W, Grün S (submitted) Saccade-related LFP modulations support synchrony of visually elicited spikes
Johnson DH (1996) Point process models of single-neuron discharges. J Comput Neurosci 3(4):275–299
Kass R, Ventura V (2006) Spike count correlation increases with length of time interval in the presence of trial-to-trial variation. Neural Comput 18(11):2583–2591
Kilavik B, Roux S, Ponce-Alvarez A, Confais J, Grün S, Riehle A (2009) Long-term modifications in motor cortical dynamics induced by intensive practice. J Neurosci 29(40):12653–12663
Kumar A, Rotter S, Aertsen A (2008) Conditions for propagating synchronous spiking and asynchronous firing rates in a cortical network model. J Neurosci 28:5268–5280
Louis S, Gerstein GL, Grün S, Diesmann M (in press) Surrogate spike train generation through dithering in operational time. Front Comput Neurosci
Maldonado P, Babul C, Singer W, Rodriguez E, Berger D, Grün S (2008) Synchronization of neuronal responses in primary visual cortex of monkeys viewing natural images. J Neurophysiol 100:1523–1532
Marsalek P, Koch C, Maunsel J (1997) On the relationship between synaptic input and spike output jitter in individual neurons. Proc Natl Acad Sci 94:735–740
Nawrot M, Aertsen A, Rotter S (1999) Single-trial estimation of neuronal firing rates: from single-neuron spike trains to population activity. J Neurosci Methods 94:81–92
Nawrot M, Aertsen A, Rotter S (2003) Elimination of response latency variability in neuronal spike trains. Biol Cybernet 88:321–334
Nawrot M, Boucsein C, Rodriguez-Molina V, Aertsen A, Grün S, Rotter S (2007) Serial interval statistics of spontaneous activity in cortical neurons in vivo and in vitro. Neurocomputing 70:1717–1722
Nawrot M, Boucsein C, Rodriguez Molina V, Riehle A, Aertsen A, Rotter S (2008a) Measurement of variability dynamics in cortical spike trains. J Neurosci Methods 169:374–390
Nawrot M, Farkhooi F, Grün S (2008b) Significance of coincident spiking considering inter-spike interval variability and serial interval correlation. In: Frontiers in computational neuroscience. Conference abstract: Bernstein symposium 2008. doi:10.3389/conf.neuro.10.2008.01.017
Palm G (1981) Evidence, information and surprise. Biol Cybernet 42:57–68
Pauluis Q, Baker SN (2000) An accurate measure of the instantaneous discharge probability with application to unitary joint-event analysis. Neural Comput 12(3):647–669
Pazienti A, Maldonado P, Diesmann M, Grün S (2008) Effectiveness of systematic spike dithering depends on the precision of cortical synchronization. Brain Res 1225:39–46
Perkel DH, Gerstein GL, Moore GP (1967) Neuronal spike trains and stochastic point processes. II. Simultaneous spike trains. Biophys J 7(4):419–440
Perkel DH, Gerstein GL, Smith MS, Tatton WG (1975) Nerve-impulse patterns: a quantitative display technique for three neurons. Brain Res 100:271–296
Pipa G, Grün S, van Vreeswijk C (under revision) Impact of spike-train autostructure on probability distribution of joint-spike events. Neural Comput
Pipa G, Riehle A, Grün S (2007) Validation of task-related excess of spike coincidences based on NeuroXidence. Neurocomputing 70:2064–2068. Published online 2006: doi:10.1016/j.neucom.2006.10.142
Pipa G, van Vreeswijk C, Grün S (in preparation) Impact of spike-train autostructure on Unitary Events
Pipa G, Wheeler D, Singer W, Nikolic D (2008) NeuroXidence: reliable and efficient analysis of an excess or deficiency of joint-spike events. J Comput Neurosci 25(1):64–88

Prut Y, Vaadia E, Bergman H, Haalman I, Hamutal S, Abeles M (1998) Spatiotemporal structure of cortical activity: properties and behavioral relevance. J Neurophysiol 79(6):2857–2874
Reyes A (2003) Synchrony-dependent propagation of firing rate in iteratively constructed networks in vitro. Nature Neurosci 6:593–599
Richmond B (2009) Stochasticity spikes and decoding: sufficiency and utility of order statistics. Biol Cybernet 100(9):447–457
Riehle A, Grün S, Diesmann M, Aertsen A (1997) Spike synchronization and rate modulation differentially involved in motor cortical function. Science 278(5345):1950–1953
Riehle A, Grammont F, Diesmann M, Grün S (2000) Dynamical changes and temporal precision of synchronized spiking activity in monkey motor cortex during movement preparation. J Physiol (Paris) 94:569–582
Rodriguez-Molina V, Aertsen A, Heck D (2007) Spike timing and reliability in cortical pyramidal neurons: Effects of EPSC kinetics input synchronization and background noise on spike timing. PLoS ONE 2(3):e319. doi:10.1371/journal.pone.0000319
Roy A, Steinmetz PN, Niebur E (2000) Rate limitations of unitary event analysis. Neural Comput 12:2063–2082
Shadlen MN, Movshon AJ (1999) Synchrony unbound: a critical evaluation of the temporal binding hypothesis. Neuron 24:67–77
Shimazaki H, Amari S, Brown E, Grün S (2009) State-space analysis on time-varying correlations in parallel spike sequences. In: IEEE international conference on acoustics, speech, and signal processing (ICASSP), pp 3501–3504
Shimazaki H, Shinomoto S (2010) Kernel bandwidth optimization in spike rate estimation. J Comput Neurosci. doi:10.1007/s10827-009-0180-4
Singer W (1999) Neuronal synchrony: a versatile code for the definition of relations?. Neuron 24(1):49–65
Softky WR, Koch C (1993) The highly irregular firing of cortical cells is inconsistent with temporal integration of random EPSPs. J Neurosci 13(1):334–350
Vaadia E, Haalman I, Abeles M, Bergman H, Prut Y, Slovin H, Aertsen A (1995) Dynamics of neuronal interactions in monkey cortex in relation to behavioral events. Nature 373:515–518
Ventura V, Carta R, Kass R, Gettner S, Olson C (2002) Statistical analysis of temporal evolution in single-neuron firing rates. Biostatistics 3(1):1–20
Ventura V, Cai C, Kass R (2005) Trial-to-trial variability and its effect on time-varying dependency between two neurons. J Neurophysiol 94(4):2928–2939
Von der Malsburg C (1981) The correlation theory of brain function. Internal report 81-2, Max-Planck-Institute for Biophysical Chemistry, Göttingen, FRG